Accepted Manuscript

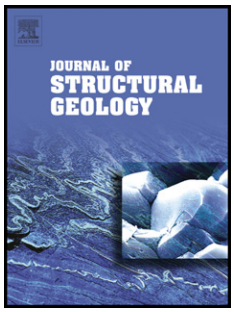

Experimental generation of volcanic pseudotachylites: constraining rheology

Yan Lavallée, Thomas M. Mitchell, Michael J. Heap, Jérémie Vasseur, Kai-Uwe Hess, Takehiro Hirose, Donald B. Dingwell

PII: S0191-8141(12)00036-3

DOI: 10.1016/j.jsg.2012.02.001

Reference: SG 2717

To appear in: *Journal of Structural Geology*

Received Date: 23 May 2011

Revised Date: 30 January 2012

Accepted Date: 1 February 2012

Please cite this article as: Lavallée, Y., Mitchell, T.M., Heap, M.J., Vasseur, Jérémie, Hess, K.-U., Hirose, T., Dingwell, D.B., Experimental generation of volcanic pseudotachylites: constraining rheology, *Journal of Structural Geology* (2012), doi: 10.1016/j.jsg.2012.02.001

Experimental generation of volcanic pseudotachylites: constraining rheology

Yan Lavallée[1†], Thomas M. Mitchell[2], Michael J. Heap[3], Jérémie Vasseur[1], Kai-Uwe Hess[1], Takehiro Hirose[4], Donald B. Dingwell[1]

[1]Earth and Environment, Ludwig-Maximilians University – LMU-Munich, Theresienstrasse 41/III, 80333 Munich, Germany

[2]Experimental Geophysics Laboratory, Institute for Geology, Mineralogy, and Geophysics, Ruhr-University, 44780 Bochum, Germany

[3]Laboratoire de Géophysique Expérimentale, Institut de Physique de Globe de Strasbourg (UMR 7516 CNRS, Université de Strasbourg/EOST), 5 rue René Descartes, 67084 Strasbourg cedex, France

[4]Kochi Institute for Core Sample Research (KCC), Japan Agency for Marine-Earth Science and Technology (JAMSTEC), 200 Monobe-otsu, Kochi, Nankoku 783-8502, Japan

[†]Corresponding author

Abstract

Volcanic systems are highly dynamic environments that comprise rocks and magmas, which, in the process of strain localisation (*e.g.*, in catastrophic flank collapse or dome-building events), are candidate materials for the occurrence of frictional melting and the formation of pseudotachylytes. We evaluate the frictional behaviour of a plagioclase-, two-pyroxene- and glass-bearing andesite and introduce an approach to constrain the rheology of frictional melts. Frictional slip at a rate of 1.3 m/s under an axial stress of 1.5 MPa induces heating at a rate approximating 130 °C per meter of slip and frictional melting of the andesite occurs at >1000 °C, which corresponds to a peak in shear stress. With continuing displacement, the shear stress decreases by ~25% from the peak strength and stabilises while the temperature equilibrates to 1230-1290 °C. The shear stress for the system is congruent with a non-Arrhenian temperature-dependent frictional melt rheology exhibiting a non-Newtonian viscosity evolving from approximately $10^{4.2}$ to $10^{3.4}$ Pa·s. Post-experiment analysis show a gradation from 1) the host rock, to 2) an extraordinary zone of unmelted, yet viscously-deformed material, to 3) a thin, outer region of chemically heterogeneous protomelts, and to 4) an inner region of chemically homogeneous frictionally generated/modified melt in the core of the slip zone. We discuss the role and identification of frictional melting in volcanic systems and the implication of viscous remobilisation of magmatic plugs during frictional slip of glass-bearing volcanic materials.

1. Introduction

In recent years, frictional melts generated in localised slip zones in faults have been shown to exert control on coseismic faulting and earthquake slip (Spray, 1987,

Hirose and Shimamoto, 2005, Di Toro et al., 2006b, Di Toro et al., 2011). During earthquakes where fault slip is localized to narrow slipping zones (at ca. >0.1 m/s), most frictional work is converted to heat; for instance, more than 1400 °C can be generated during seismic slip events along slip zones thinner than 10 mm if the shear strength remains constant (*e.g.*, Rice, 2006). Such temperature increases are sufficient to melt the wallrocks along the slip zone, producing frictional melts which cool to form a pseudotachylyte (Sibson, 1975), which is often used to infer seismic fault motion on exhumed faults (Cowan, 1999).

Melting of rocks under such rapid-heating events is perceived to be a non-equilibrium thermodynamic process (Spray, 1992) in which selective melting of individual crystal phases depend on their fusion temperatures (Lin and Shimamoto, 1998). Sustainability of slip and friction (along a discrete slip plane) regulate melting and the retreat of the rock-melt interface along seismogenic faults – a thermodynamic phenomenon described as a Stefan problem (Hirose and Shimamoto, 2005). As melting ensues, the chemical composition of the melt evolves, which is an additional factor controlling the shear resistance of faults coated by frictional melts (Hirose and Shimamoto, 2005). The shear resistance of the viscous layer is determined by the viscosity and shear strain rate of the molten layer, previously approximated as a Newtonian liquid with Arrhenian temperature dependence of viscosity (*e.g.*, Spray, 1993, Ujiie et al., 2007, Piccardo et al., 2010). Frictional melts may act as lubricants to seismic motion as strong velocity-weakening of faults occurs during melt generation, which has a significant effect on the frictional properties in slip zones (Di Toro et al., 2006a). When a molten layer separates a fault during seismic slip, it is no longer rock-to-rock friction but viscous energy dissipation that becomes the heat source. During deceleration and cessation of slip, the heat generated by friction

dissipates into the surrounding country rocks and the melt succumbs to one of two fates: 1) crystallization or 2) quenching to a glass, both preserved henceforth, in the geologic record, as pseudotachylytes. But dynamically, how do frictional melts evolve? And equally important, what are the rheological consequences of chemically evolving frictional melts on the frictional properties of slip zones?

The most common rock-forming minerals are silicates and as such, frictional melting results primarily in the generation of silicate melts. Initial melting events, although a non-equilibrium process, mix and reach equilibrium with slip (Hirose and Shimamoto, 2005). Chemical mixing of silicate melts is controlled by diffusion and convection (Mezic et al., 1996, Perugini and Poli, 2004, Perugini et al., 2010). During non-equilibrium frictional melting, slip forces convection. This action stretches the interface between melt batches (from selective melting) and increases the surface area available for chemical diffusion, thereby enhancing the efficiency of chemical homogenization. The chemical composition of a melt strongly influences the rheology of silicate melt (Dingwell and Webb, 1989). The viscosity of silicate liquids has been extensively studied in the Newtonian region for a range of compositions (Murase and McBirney, 1970, Bottinga and Weill, 1972, Shaw, 1972, Dingwell et al., 1985, Persikov et al., 1990, Dingwell, 1991, Yue and Brückner, 1994, Dingwell et al., 1996, Hess and Dingwell, 1996, Richet et al., 1996, Scaillet et al., 1996, Dingwell et al., 1997, Dingwell and Hess, 1998, Schulze et al., 1999, Liebske et al., 2003, Sato, 2005, Malfait et al., 2011), including mineral compositions (Cukierman and Uhlmann, 1973, Cranmer and Uhlmann, 1981, Richet, 1984, Tauber and Arndt, 1987, Neuville and Richet, 1991, Taniguchi, 1992, Askarpour et al., 1993, Toplis et al., 1997, Schilling et al., 2001): it is known to exhibit a strong non-Arrhenian temperature dependence and recent models for its estimation are reasonably accurate over a wide range of

94 geochemical compositions (Hui and Zhang, 2007, Giordano et al., 2008). The onset of
95 non-Newtonian rheology in melts is also well-documented empirically (Li and
96 Uhlmann, 1968, 1970, Simmons et al., 1982, Simmons et al., 1988, Dingwell and
97 Webb, 1989, 1990, Brückner and Yue, 1994, Simmons, 1998) and found to correlate
98 with strain rates approaching the relaxation rate of the liquid structure (to within 3
99 orders of magnitude; *e.g.*, Webb and Dingwell, 1990). In the case of partially molten
100 rocks, such as those produced by frictional slip, the presence of crystals and bubbles
101 may also affect the rheological properties both by influencing the Newtonian (static)
102 suspension viscosity and by the addition of strain-rate dependence (Bagdassarov and
103 Dingwell, 1992, Stein and Spera, 1992, Bagdassarov et al., 1994, Lejeune and Richet,
104 1995, Stevenson et al., 1996, Lejeune et al., 1999, Stein and Spera, 2002, Caricchi et
105 al., 2007, Lavallée et al., 2007, Cordonnier et al., 2009). Frictional melting thus
106 results in the generation of a complex, disequilibrium multiphase magma with the
107 result that its rheological properties are almost unknown. The frictional properties of
108 faults which produce complex frictional melts are thus intimately linked to the
109 chemical and physical evolution of the melt.

110 To date, frictional melting experiments have been conducted primarily on
111 intrusive, metamorphic and sedimentary rocks (Spray, 1987, 1988, Kennedy and
112 Spray, 1992, Shimamoto and Lin, 1994, Spray, 1995, Tsutsumi and Shimamoto,
113 1997, Hirose and Shimamoto, 2005, Di Toro et al., 2006a, Di Toro et al., 2006b,
114 Tsutsumi and Mizoguchi, 2007, Del Gaudio et al., 2009, Sato et al., 2009, Ujiie et al.,
115 2009, Kim et al., 2010, Niemeijer et al., 2011). The majority of these studies focus on
116 the control of frictional melts on coseismic earthquake dynamics of seismogenic
117 crustal-scale faults, which commonly initiate near the brittle-ductile transition at some
118 ca. 10-km depth. Volcanic regions, however, with their ambient temperatures above

that of the typical crustal geotherm (for a given depth) as well as their perpetually deforming nature stand as ideal candidates for frictional melting and formation of pseudotachylytes. Yet, the potential for frictional melting in this geological setting as well as the frictional properties of volcanic rocks has been, to date, unexplored.

Volcanic systems are dynamic environments, which are highly seismogenic. Magma ascent and eruptions are accompanied by complex seismic signal trigger mechanisms ranging from failure of conduit wallrocks and magma, to frictional slip and degassing (e.g., Sparks, 2003). In recent years, magma has been increasingly recognised as a seismic source triggered by strain localisation, leading to fracturing and subsequent slip (*e.g.*, Iverson et al., 2006, Neuberg et al., 2006, Johnson et al., 2008, Lavallée et al., 2008, Tuffen et al., 2008). The role and extent of friction-controlled ascent in conduits has been quantified with regard to viscous flow (*e.g.*, Melnik and Sparks, 1999, Costa et al., 2007, Melnik et al., 2009), stick-slip behaviour (*e.g.*, Tuffen et al., 2003, Neuberg et al., 2006, Melnik et al., 2009), cataclastic flows of gouge material (*e.g.*, Cashman et al., 2008, Kennedy et al., 2009, Kennedy and Russell, 2011), ejections of pyroclasts during explosive eruptions (*e.g.*, Wilson et al., 1980, Ramos, 1995, Bower and Woods, 1996), and recently with regard to frictional melting (*e.g.*, Kendrick et al., this issue). In fact, to our knowledge, only five studies exist evaluating pseudotachylytes in volcanic systems: including the aforementioned study of frictional melting in volcanic conduit, complementary studies have also alluded to the occurrence of frictional melting in a sector collapse (Legros et al., 2000), in pyroclastic/block-and-ash flows (Grunewald et al., 2000, Schwarzkopf et al., 2001) and in caldera subsidence-controlling faults (Kokelaar, 2007).

Volcanic rocks (in contrast to intrusive, sedimentary and metamorphic rocks) present an additional complexity in that their groundmass commonly comprises an

144 initial fraction of interstitial glass. Glass does not form via a phase transition in the
145 Gibbsian thermodynamic sense, rather, liquid and glassy melts are two physical states
146 of the same phase, discriminated by strain rate and temperature (Dingwell and Webb,
147 1989). The ability of silicate melts in magmas, to switch from a liquid to a glassy state
148 (and back) is well described by a Maxwell body viscoelasticity with a transition
149 known as T_g, the glass transition (Webb and Dingwell, 1990). T_g is a kinetic barrier,
150 dependent predominantly on chemical composition and temperature; it typically
151 occurs at a temperature hundreds of degrees below the melting point in simple
152 congruently melting systems and often well below the range of crystallisation in
153 magmas. Volcanic rocks preserving the glassy groundmass phase may thus be
154 remobilised to viscous liquids at temperatures well below their melting temperatures
155 or those of their constituent phases. Thus the remobilisation of pseudotachylyte in
156 volcanic systems forms a special material case with potentially surprising
157 characteristics. Understanding the frictional properties of volcanic rocks subject to
158 selective melting and formation of volcanic pseudotachylyte may greatly improve our
159 ability to predict the flow and strain localisation observed in volcanic domes and
160 inferred for volcanic conduits. As such flow models are an essential ingredient of
161 reliable interpretation of volcano monitoring signals, the mitigation of volcanic
162 eruptions stands to gain from a better understanding of the role of frictional melting
163 and pseudotachylyte development in volcanic environments. Here, we introduce a
164 method which combines frictional, geochemical and rheological data to constrain the
165 rheology of frictional melts and present results from a high-velocity rotary experiment
166 on a glass-bearing andesitic rock to evaluate the role and generation of
167 pseudotachylyte in volcanic environments.
168

2. Methodology

2.1. Experimental procedure

This study targets subduction-related, volcanic arc environments and most specifically, a glassy volcanic rock to evaluate the influence of glass on the mechanical response of rocks during slip in comparison with the exclusively crystalline lithologies investigated to date (*e.g.*, Hirose and Shimamoto, 2005, Di Toro et al., 2006b, Del Gaudio et al., 2009). To this end, a fresh andesite rock erupted in 2004 at Volcán de Colima (Mexico) was chosen, as it is an intermediate volcanic rock, typical of stratovolcanoes and dome-building eruptions. The andesite sample used in this study optically contains about 80% crystals (40 vol.% phenocrysts and 40 vol.% microlites) and 20 vol.% interstitial glass (and 8 vol.% porosity, based on He-pycnometry). The assemblage comprises 60 vol.% plagioclase, 14 vol.% orthopyroxene, 10 vol.% clinopyroxene, 5 vol.% titanomagnetite, and occasional crystals of hornblende and olivine (See also Reubi and Blundy, 2008, Savov et al., 2008). This andesite is anhydrous and was erupted as a volatile-poor lava (Reubi and Blundy, 2008), which simplifies the description of the melting process as well as the evolution of the viscosity (*c.f.*, Hess and Dingwell, 1996).

Frictional melting was experimentally investigated using a high-velocity rotary apparatus at the Kochi Core Center in Japan (Fig. 1, see Hirose and Shimamoto, 2005, for details of the technique). To this end, we prepared plane-parallel cylindrical samples (with a diameter of 24.94 mm and a length of 20 mm), one of which is held stationary and has axis-parallel drill holes to permit the insertion of four K-type thermocouples (1.1, 1.3, 3 and 5 mm away from the slip zone; see Fig. 1b), and the other which is placed in the rotary side of the loading column. The sample pair was placed at position 1 in the apparatus (see Fig. 1) and an axial stress of

194 1.5 MPa (equivalent to a depth of ~65 m) was applied from the stationary side by
195 means of an air actuator. The experiment was conducted at slip velocity of 1.3 m/s
196 until the shear stress attains nearly steady-state value, so as to ensure the quasi-
197 isothermal state of the partial melt and thus allow the quantification of the end
198 products.
199
200 *2.2. Temperature correction*
201 In the case of rapid heating which accompanies high-velocity friction, the
202 temperature monitored in the host rock only provides an approximation of the actual
203 temperature at the slip interface; in fact, the thermocouple reads the temperature
204 dissipated through time. It thus result that each read temperature increments were
205 experienced at the slip interface at an earlier time. We assume a semi-infinite 1D
206 medium undergoing thermal conduction without dissipation, following the heat
207 equation (*e.g.*, Nielsen et al., 2008):

208 $$-\frac{\partial^2 T}{\partial x^2} = \frac{1}{\kappa}\frac{\partial T}{\partial t} \qquad \text{with: } \begin{cases} T(x, t=0) = T_0 \\ T(x=0, t) = T_c \end{cases} \qquad (1)$$

209 which includes a uniform initial temperature T_0 of the medium and upon slip and
210 heating, imposes a temperature T at the interface (using a Dirichlet boundary
211 condition which averages the imposed fix temperature at each time interval). κ is the
212 thermal diffusivity of andesite approximated as 5.3×10^{-7} m^2/s (Labaš et al., 2006) and
213 T_c is the temperature measured by the thermocouple at a distance monitored during
214 the experiment. We apply a change of variable $\overline{T} = T - T_0$ to equation 1 in order to
215 extract the temperature at a position x, thus obtaining:

216 $$-\frac{\partial^2 \overline{T}}{\partial x^2} = \frac{1}{\kappa}\frac{\partial \overline{T}}{\partial t} \Leftrightarrow -\frac{\partial^2 \overline{T}}{\partial x^2} - \frac{1}{\kappa}\frac{\partial \overline{T}}{\partial t} = 0 \qquad \text{with: } \begin{cases} \overline{T}(x, t=0) = 0 \\ \overline{T}(x=0, t) = T_c - T_0 \end{cases} \qquad (2).$$

This heat equation can be solved using the following Laplace transform:

$$\theta(x,p) = L\{\bar{T}(t)\} = \int_0^\infty \exp(-pt)\bar{T}(x,t)dt \quad (3)$$

which, once applied, provides us with

$$-\frac{d^2\theta}{dx^2} - \frac{1}{\kappa}\left(p\theta - \bar{T}(x,t=0)\right) = 0 \Leftrightarrow -\frac{d^2\theta}{dx^2} - q^2\theta = 0 \qquad \text{with: } q^2 = \frac{p}{\kappa} \quad (3)$$

offering a mathematical solution of the type $\theta(x,p) = -(A\exp(-qx) + B\exp(qx))$. The temperature keeps a finite value when x goes towards infinity, so that $B = 0$ and

$$\theta(x,p) = -A\exp(-qx) \text{ with } \theta(x=0,p) = A = \frac{T_c - T_0}{p}.$$

Finally the use of Laplace inverse transform leads to:

$$T(x,t) - T_0 = \theta(x,p) = -(T_c - T_0)\frac{\exp(-qx)}{p} = -(T_c - T_0)\,\mathrm{erf}\left(\frac{x}{2\sqrt{\kappa t}}\right) \quad (4)$$

and therefore

$$T(x,t) = T_0 - (T_c - T_0)\,\mathrm{erf}\left(\frac{x}{2\sqrt{\kappa t}}\right) \quad (5)$$

which is used to approximate the temperature along the slip interface. This estimation, although simplistic in its discretisation of time and temperature intervals, appears to satisfactorily approximate the evolution of temperature during slip, since the modelled temperatures initially diverge from the thermocouple read out (while heating takes place faster than what is recorded), then converge as the sample shortens and the thermocouple approaches and intrudes the melt zone (henceforth providing an *in-situ* measurement of the melt temperature). The thermal constraint has obvious implication for the mechanics experienced at the slip zone. Yet, a more accurate three-dimensional derivation of the temperature evolution via the forward iteration of

239 an analytical solution to Fourier's law of conduction applied to a cylinder is beyond
240 the scope of this study and will require attention in future studies in order to fully
241 integrate rheological constraints to the mechanics of slip in the presence of frictional
242 melts.
243
244 *2.3. Structural, physical and chemical imaging*
245 Structural description of the slip zone was performed using backscattered
246 electron images, taken with a CAMECA SX100 electron probe micro analyser
247 (EPMA) equipped with wavelength dispersive spectrometers as well as backscattered
248 electron imaging (BSE) capability at the LMU-Munich. Image intensities – that is,
249 variations in grey scales as a result of molecular densities of each phase – were taken
250 at 15kV and allowed us to distinguish between melt batches as well as to identify the
251 distribution and shape of partially molten crystal fragments. Calibration of the
252 intensity spectrum of each phase was achieved by electron microprobe analysis (see
253 section 2.4). The shape and fraction of phases were estimated using the intensity
254 spectrum in the 0-255 grey scale, as an input parameter in the free, online image
255 analysis toolbox JMicroVision 1.2.7 (Roduit, 2006).
256 3-D high-resolution images were acquired via a v/tome/x s 240 micro-CT
257 scanner from General Electric (Phoenix) using a high-power X-ray tube and a drx-250
258 rt detector system. The scans were acquired at a voltage of 120 kV and a current of
259 167 nA for an exposure time of 1 s, cumulating 2000 images for 360° (Vsensor 2
260 mode), which provided a Pixel/Voxel size resolution of 14.78 μm.
261
262 *2.4. Geochemical analysis*

The geochemical composition of the frictional melt was measured for major and minor elements using the same EPMA. The measurements were performed on glass (*i.e.*, the frictional 'melt') with a 10 μm defocused beam set at 10 nA (Table 1).

2.5. Thermal analysis

The heat capacity of the frictional melt was determined in a Netzsch DSC-404C differential scanning calorimeter (DSC). Here, ~20 mg of glass fragments, prepared from the frictional melt expelled, were heated in the DSC at a rate of 10 ºC/min until crossing of T_g, which is evidenced by a peak in heat capacity. The material was subsequently cooled and reheated, both under the same rate of 10 °C/min, to established the actual T_g of the liquid, which for such a known rate is equivalent to ~10^{11} Pa·s (*e.g.*, Gottsmann et al., 2002) and serve to constrain the accuracy of temperature-dependence of viscosity (modelled in section 2.6).

2.6. Frictional melt viscosity

The viscosity of the multiphase melt present in the slip zone was modelled in five steps:

(1) The non-Arrhenian temperature-dependence of the viscosity of the frictional melt was estimated using the measured chemical composition as an input parameter in the most up-to-date, web-based GRD viscosity calculator (available online at http://www.eos.ubc.ca/~krussell/VISCOSITY/grdViscosity.html), which is modelled on a Vogel-Fulcher-Tamman equation:

$$\eta = \mathrm{A} + \frac{\mathrm{B}}{\mathrm{C} + \mathrm{T}} \qquad (6)$$

where the relationship between viscosity (η in Pa·s) and temperature (T in Kelvin) is dependent on the A, B, and C, which are parameters modelled using 1770 viscosity

288 measurements on a wide range of geochemical compositions (Giordano et al., 2008).
289 In the estimates presented in this study, zero water and fluorine contents are assumed,
290 based on the absence of hydrous phases and on the conclusion from Reubi and
291 Blundy (2008) and Savov *et al.* (2008) that this andesite was dry upon eruption.
292 (2) The viscosity-temperature relationship was compared to the calorimetric
293 estimation of the viscosity at the T_g interval in order to validate the use of the GRD
294 viscosity calculator and see whether the frictional melt is chemically homogenized
295 and evidence only one T_g peak or is not chemically mixed and evidence multiple T_g
296 peaks.
297 (3) The rheological effects added by the presence of crystals were estimated, using the
298 empirical/analytical, relative-viscosity calculator of Costa and others (Costa et al.,
299 2009; available online at http://datasim.ov.ingv.it/~costa/#Articles):

300 $$\eta_{\mathrm{r}}(\Phi)=\frac{1+(\frac{\Phi}{\Phi_*})^{\delta}}{\left[1-\mathrm{F}(\frac{\Phi}{\Phi_*},\xi,\gamma)\right]^{\mathrm{B}\Phi_*}} \quad (7)$$

301 $$\mathrm{F}=(1-\xi)\mathrm{erf}\left[\frac{\sqrt{\pi}}{2(1-\xi)}\frac{\Phi}{\Phi_*}\left(1+\frac{\Phi^{\gamma}}{\Phi_*^{\gamma}}\right)\right] \quad (8)$$

302 where $\eta_r(\phi)$ is the relative viscosity increase due to the crystal fraction (ϕ) which is
303 estimate at 0.3 in the experiment (see Cimarelli et al., 2011, for the rectified
304 formulation of the equations). As input parameter, we used 0.56 as a critical solid
305 fraction (ϕ_*) for the nearly equant and equigranular crystal population developed in
306 the frictional melt, 2.5 for the Einstein coefficient (B) and ξ and γ, are empirical
307 geometrical relationship with strain rate, which were solved by Carrichi *et al.* (2007)
308 and are included in the relative-viscosity calculator by Costa *et al.* (2009).

(4) The strain rate ($\dot{\varepsilon}$) of the melt within the slip zone was estimated by using the rate of rotation (ν), perimeter of the circular trajectory at a given radius (0<*r*<12.48 mm) in the sample interface (averaged to 6.24 mm for the purpose of the calculation) and the thickness of the slip zone (*d,* equivalent to zone 3 & 4), which after cooling (and after some compression by the apparatus) vary from 0.4 in the middle to 0.6 near this outer margin (Fig. 3e), which provide a minimum estimate averaged at *d*≈ 0.5 mm:

$$\dot{\varepsilon} = \frac{2\pi r}{\nu d} \quad (9)$$

In this analysis, the melt is assumed not to slip along the rock boundary, which concurs with the irregular geometry of crystal fragments at the slip surface.

(5) The evolution of viscosity during slip is finally modelled as a function of the corrected temperature (modelled on the basis of the recorded temperature profile). This estimation is provided to a first order without considering rheological complexities undergone as crystals, melt and protomelts (*i.e.*, initial selective melt chemically reflecting the local crystal assemblage) chemically homogenize, since the timescale for assimilation and mixing are not included here and will be the subject of a future study. Following this overlapping of empirical models used in our viscosity calculation, we estimate the accuracy of the modelled values to +/-0.2 logarithmic units of viscosity.

3. Mechanics, dynamics and microstructure of high-velocity frictional melts

High-velocity friction experiments of the andesitic rock were characterized by an abrupt increase in shear stress, followed by a minor decrease in the first metre of slip (Fig. 2 inset). With increasing slip, the shear stress gradually increases while the temperature rapidly increased on the order of ~100 °C per meter of slip (modelled to ~130 °C/m), and a growth of glowing patches on the slip plane is seen after ~8 m of

slip (Fig. 2). This strengthening is due to the melt patches growing into a thin continuous layer which extends across the entire slip zone after 12 m of displacement, corresponding with the second friction peak. From this point on, a second weakening phase began, which is due to a growth of the molten layer resulting in the reduction in the shear stress (Hirose and Shimamoto, 2005). This phase of frictional melting was accompanied by continuous axial shortening of the sample at a rate of 0.43 mm/s in addition to a continued rise in temperature (recorded for as long as the thermocouple did not break due to sample shortening) and expulsion of the pervasive melt (Fig. 3a).

Optical analysis of the slip zone under the microscope, showed a gradation from (Fig. 3b): (#1) intact host rock 2.5 mm from the edge of the slip zone (Fig. 3c) to (#2) a thin zone of increased crystal mobility between 2.5 and 0.4 mm (Fig. 3d), (#3) a thin sheared zone of partially molten rocks between 0.4 and 0.3 mm, and (#4) a ~0.2- to 0.4- mm thick zone of melt containing resorbed, equant crystal fragments primarily of plagioclase with some pyroxenes as well as spherical opaque droplets and micro-bubbles (Fig. 3e, 4).

BSE and X-ray CT imaging provide a clear view of the physical and chemical heterogeneities developed in the slip zone. All four zones described above were identified. Furthermore, the slip zone hosts cracks, which crosscut all four zones (Fig. 4a). X-ray computed tomographic imaging reveals 3-dimensional details of the slip zone (Fig. 5). Zone #3 shows that frictional melting mainly initiated in the outer part of the sample, whereas the core retained coarser, unmelted crystals. Slip also developed ring structures, with variable bubble concentrations (Fig. 5b). The crosscutting cracks observed under BSE are also visible under X-ray. These cracks are best developed in zone #4, showing a network of radial and concentric cracks in the frictional melt, suggesting propagation of the crack caused by contraction during

359 cooling (a phenomenon not necessarily taking place in nature owing to slow cooling
360 of large body masses).

361 The onset of selective melting preserved in the outer margin of zone #3
362 revealed batches of protomelts with different chemical compositions (Table 1). One
363 melt pocket had the composition of a single crystal whereas others have the
364 composition of different ratios of plagioclase to pyroxene (*e.g.*, Glass #10, #11, #54
365 and #55; Table 1). In our search for different protomelts, we did not find pure
366 pyroxene melt pockets. The protomelts are intertwined in a chaotic manner and blend
367 where they pinch into one another (Fig 4b); they show varying degrees of mixing. In
368 the slip zone #4 and in the expelled melt, the BSE images reveal the presence of a
369 chemically homogeneous frictional melt phase hosting droplets of iron oxides and a
370 suspension of plagioclase and pyroxene fragments. The frictional melt zone
371 essentially is chemically equivalent to that of the bulk rock analysis (Table 1).

372 The intensity spectrum of each phase was determined on five BSE images
373 taken in zone #4 (Fig 4c), using the grey scale range 82-94 for the frictional phase,
374 126-255 for the iron oxides droplets, 40-81 for the plagioclase, 95-125 for the
375 pyroxene and 0-39 for bubbles as input parameter in JMicroVision. This grey scale
376 bracketing identified 3688 entities (n) and constrained 27 vol.% plagioclase (n =
377 1822), 3 vol.% pyroxene (n = 2), 9 vol.% iron oxides droplets (n = 1217) and 1 vol. %
378 bubbles (n = 364), leaving an additional 60 vol.% of frictional melt. This was
379 complemented by image analysis of the expelled melt which yielded equivalent
380 values, highlighting the steady-state character of the frictional process.

381

382 **4. Constraining the rheology of frictional melts**

383 The viscosity of frictional melts can be approximated, to a first order, using
384 empirical equation based on their chemical composition. The presence of chemically
385 heterogeneous protomelt pockets in zone #3 implies that the viscosity may widely
386 vary at a microscopic scale (Fig. 6a). In the slip zone, however, the homogeneous
387 composition of the frictional melt nears equilibrium with its mineral assemblage [see
388 comparison of frictional melt and bulk rock data (Table 1)] and thus permits the use
389 of a well-defined, non-Arrhenian temperature (T in Kelvin)-viscosity (η in
390 Pa·s) relationship modelled as:

391 $$\mathrm{Log}\eta = -4.55 + \frac{8044.9}{\mathrm{T} - 747.5} \qquad (10)$$

392 When comparing values obtained through this equation with the measured
393 calorimetric T_g of 690 ºC (Fig. 6b-c), we observe that the T_g agrees with the frictional
394 melt viscosity of 10^{11} Pa·s. This agreement and the observation of a single T_g peak
395 imply that the bulk of frictional melt reached overall chemical and structural
396 homogeneity. Indeed, the minor proportion of protomelts to frictional melt supports
397 the use of the latter in our calculation of suspension viscosity.

398 The apparent viscosity of the suspension generated by frictional melting was
399 modelled by adding the relative effects of crystals (estimated using Costa et al., 2009)
400 to the modelled viscosity equation 10 (Fig. 6c). In this calculation we couple both
401 plagioclase and pyroxene as solid particles (30 vol.%), whereas we consider the iron
402 oxides as part of the interstitial melt, due to their ability to deform viscously (at
403 extremely low viscosity of ~10^{-2} Pa·s). [Note: bubbles were too few and spread to
404 yield strong rheological consequences and as such they were not considered in the
405 calculation.] The presence of 30 vol.% of near equant crystal fragments adds
406 approximately 0.71 order of magnitude of viscosity. During the experiment however,
407 thickening of the frictional melt layer (from 0 to ~0.5mm) and variable strain rate

across the slip zone (0 to $2.6x10^3$ s^{-1}) thus promote a gradient in the relative viscosity increase of the shear thinning suspension from about 0.71 in the middle of the sample to 0.45 at the outer margin (with an average of 0.58). Computation of the viscosity progression using the modelled temperature of the slip zone (assuming it is homogeneous) shows that the viscosity estimates decreased from $10^{4.2}$ to $10^{3.4}$ Pa·s and remained around this value after complete spreading of the melt layer at the slip interface (Fig. 6d), which led to the 25% decrease in shear stress before stabilisation and establishment of a thermal and kinetic balance. Under such a high slip rate, and therefore strain rate, the frictional melt, with such low modelled viscosity is not expected to achieve fragmentation (by exceeding the limiting viscous relaxation rate of the structure); yet, if failure did take place, the high relaxation rate of such a low modelled viscosity would promote immediate relaxation and healing of the fragments to a fully viscous frictional melt.

5. Discussion

5.1. The complex rheology of frictional melts

The physico-chemical complexity of the process of frictional melting yields an equally complex rheological response. The estimation of natural frictional melts' viscosities, with the crystallisation overprints onto the original composition of the interstitial melt, certainly is a difficult task (*e.g.*, Spray, 1993), but with experiments, as demonstrated in this study, quenching to a glass ensures the exact rheological characterisation of the interstitial frictional melt. Since earlier attempts at modelling the viscosity of frictional melts (*e.g.*, Spray, 1993), the description of silicate liquid viscosity has much improved, with the agreement that silicate liquids are (under strain rate lower than the relaxation rate of their structure) Newtonian fluids that exhibit a

433 non-Arrhenian temperature dependence (e.g., Dingwell, 2007, and references therein).
434 Whereas earlier Arrhenian models (e.g., Bottinga and Weill, 1972, Shaw, 1972) may
435 describe well the viscosity of initial selective (*i.e.*, high-temperature) melts, non-
436 Arrhenian models (*e.g.*, Giordano et al., 2008) entails a faster than exponential
437 increase of the viscosity with cooling, which may carry drastic consequences for slip
438 cessation during heat dissipation, forcing an earlier halt.

439 The rheology of frictional melt is further influenced by the ubiquity of
440 fragments and bubbles. The description of suspension rheology has long been a
441 challenge (Einstein, 1906, 1911). In the presence of a rigid load, the physical
442 interactions of the crystals and the rock fragments augment the static viscosities
443 (Roscoe, 1952) and induce a departure from a simple Newtonian behaviour
444 (Bagdassarov et al., 1994), whereby the apparent viscosity becomes strain rate
445 dependent (*e.g.*, Caricchi et al., 2007, Lavallée et al., 2007). Unlike previous attempts
446 to estimate the rheological contribution of fragments in frictional melts based on
447 polymeric suspensions (Spray, 1993, Ujiie et al., 2007), silicic suspensions have a
448 different rheological behaviour that deserves separate consideration (*e.g.*, Costa et al.,
449 2009). The thixotropic nature of multiphase silicate melt with an apparent viscosity
450 decreasing with increase strain rates suggests that during slip cessation, reduction in
451 strain rate would promote a rapid increase in apparent viscosity, which (like the
452 aforementioned non-Arrhenian cooling scenario) may force slip to a halt. Such
453 viscous break cannot be accounted for in earlier viscosity descriptions (Spray, 1993,
454 Hirose and Shimamoto, 2005, Ujiie et al., 2007, Nielsen et al., 2008), based on
455 Arrhenian models for Newtonian suspensions. In the presence of bubbles, the
456 viscosity of liquids becomes difficult to estimate (with current models) as, depending
457 on the strain rate and whether the bubbles may remain rigid or deform, the apparent

458 viscosity of the suspension may increase or decrease, respectively (Bagdassarov and
459 Dingwell, 1992, Stein and Spera, 1992). It results that for the very low modelled
460 viscosities of frictional melts as well as their high slip (*c.f.*, strain) rates, bubbles are
461 believed to deform and thus their presence would decrease the apparent viscosity of
462 the melt, unlike previous inferences (Ujiie et al., 2007).

463 In the experiment, slip under steady state shear stress and viscosity reflects the
464 balance between melt generation, homogenisation, viscous energy dissipation versus
465 heat loss to the host rock and the surrounding, and melt extraction (e.g., Nielsen et al.,
466 2008). Difficulty however arises when quantifying the extent of viscous energy
467 dissipation since the strongest viscous heating takes place at the outer margin of the
468 samples where the slip rate is highest (since the rate of heat production scale to the
469 viscosity and the square of strain rate; Gonnermann and Manga, 2007), which is the
470 region where frictional melt is first extracted. Consequently, contribution from
471 viscous energy dissipation may be most significant in the sample's middle regions
472 where strain rates are intermediate and we estimate that heat is produced at a rate of
473 degrees per seconds if heat is not loss (Hess et al., 2008); yet the modelled
474 temperature reveal a stable temperature at the slip interface following the second peak
475 in shear stress. In nature, the contribution from viscous energy dissipation may be
476 significant (*e.g.*, Cordonnier et al., in press) and deserve further consideration in
477 future studies.

478

479 *5.2. Frictional melting in volcanic environments*

480 Volcanic environments, with their high ambient temperatures may play host to
481 frictional melting in faults where the relative temperature increase required for
482 melting is smaller than that found elsewhere in the crust where more typical crustal

483 geotherms are located. It is commonly inferred that pseudotachylytes resulting from
484 frictional melting indicate high-velocity slip (*e.g.*, 0.1 m/s) associated with earthquake
485 events (*e.g.*, McKenzie and Brune, 1972, Sibson, 1975). Such conditions are certainly
486 commensurate with the idea of pseudotachylytes in dome-building eruptions, as both
487 crystal-rich magma (behaving elastically on short timescale) and rocks (whether
488 hosting glass in the groundmass or not) reside at high temperatures (*e.g.*, 500-1000
489 °C) and thus relatively little friction is required to raise the temperature beyond the
490 mobilisation point (*i.e.*, T_g), as evidenced by the extraordinary viscous behaviour of
491 the thick zone #2 wallrock in the experiment. Kendrick *et al.* (this issue) suggest that
492 during extrusion of a ca. >730 °C spine at Mt. St-Helens, two small-magnitude 3.3
493 and 3.6 long-period earthquakes may have been associated with approximately 5-m
494 slip events, which led to remelting of the ascending crystal-rich magma. Although the
495 study of Kendrick (this issue) is the first to introduce frictional melting as a
496 mechanism regulating the ascent of high-viscosity magma in volcanic conduits, it
497 may be a common process. Difficulty may however arise in the identification of
498 pseudotachylytes in conduit margins – zones infamous for their high shear rates – due
499 to the presence of fine-grained, resorbed crystals and interstitial glass, the occurrence
500 of flow banding and the potential thermal contribution from viscous energy
501 dissipation. Also, the high ambient temperature may promote slow cooling and
502 sufficient time for recrystallization, resulting in coarse grained pseudotachylytes. Yet,
503 their distinction may be possible via 1) calorimetric analysis of the glass transition, 2)
504 geothermobarometric analysis of the crystal stability field, 3) identification of droplets
505 of iron oxide (commonly immiscible in silicate melts at low pressures) with single-
506 domain to pseudo-single-domain magnetite and 4) contrasting Curie temperatures
507 (*e.g.*, Nakamura et al., 2002). These analyses must ultimately indicate contrasting P-T

equilibrium, magnetic properties (remanence, susceptibility and domain state) and cooling history (isotropic crystal size distribution and interstitial melt content) between the wallrock and the pseudotachylyte.

Frictional melting may play an important role in the evolution of lava domes, where strain localisation and rapid dislocation of the deeper structures may remobilise and destabilise the domes. One of the most spectacular, contemporary manifestations of strain localisation takes place every hour at Santiaguito volcano (Guatemala) where sudden destabilisation along the conduit wall triggers rings of gas-and-ash explosions (Johnson et al., 2008). This activity accompanies the rapid structural uplift of the dome at an approximate rate of 0.2-0.5 m/s – a rate presumably sufficient to induce significant frictional heating. Efforts should be made to identify their importance as well as assess their contribution to volcanic flow dynamics.

Volcanic rocks commonly contain primarily plagioclase and pyroxene and/or amphibole as their main phenocrysts assemblage. In the present study, the use of an andesite bearing plagioclase and pyroxenes (that have similar melting temperatures) favoured assimilation and homogeneity of the frictional melt composition – equivalent to the chemical composition of the bulk rock. It is also possible that the similar melting temperature of the minerals resulted in a minimal fraction of fragments remaining in the melt, thereby decreasing their relative rheological contribution. In contrast, friction in andesite bearing plagioclase and amphibole – *i.e.*, minerals with contrasting melting temperatures – would result in a dichotomy at the rock-melt interface, with preferential melting of amphibole and longer resistance of plagioclase, engulfed as particles in the frictional suspension.

In the modelling of suspension rheology, the use of empirical viscosity models such as that of Costa and others (2009) may show a certain degree of discrepancy

with the actual rheology of the melt as it is built on viscosity data for a range of strain rates adequate for magmatic processes, but considerably slower than that taking place in the friction experiments or in nature, during seismogenic faulting and pseudotachylyte generation. [Yet, it is to date, the best approximation of the rheology of frictional melts.] Perhaps in the future apparatus such as the high-velocity rotary shear apparatus may be adapted to permit controlled (*i.e.*, without mass loss and crystal comminution) rheological work at such extreme conditions and complement tests on viscoelastic properties (*e.g.*, Hessenkemper and Brückner, 1991, Webb, 1991, Bornhoft and Brückner, 1994, Vo-Thanh et al., 2005). Certainly, the properties of frictional melt and their importance in modifying volcanic processes deserve an important consideration in future assessment of volcanic scenarios.

6. Summary

The rheological significance of frictional melting and pseudotachylyte generation in volcanic systems is introduced and described using a high-velocity rotary shear experiment on an andesitic volcanic rock (containing plagioclase and pyroxenes as phenocrysts and microlites as well as interstitial glass) along with a method to compute the complex strain-rate-dependent viscosity of the suspension produced during frictional melting. Rheologically, four zones are identified which grade from (#1) intact material at beyond 2.5 mm from the slip zone to (#2) a thin zone of increased crystal mobility between 2.5 and 0.4 mm due to the crossing of the glass transition temperature in the wallrocks and slow viscous deformation, (#3) a thin zone of partially molten rocks with chemically heterogeneous protomelts at ca. 0.4-0.3 mm, and (#4) a 0.2- to 0.4-mm thick zone of chemically homogeneous melt containing resorbed, equant crystal fragments as well as spherical iron oxide droplets

and micro-bubbles. Computation of the viscosity of the fictional melt indicates a transient viscosity decrease towards the outer margin of the sample. When comparing the evolution in viscosity due to heating after formation of a pervasive melt layer in the slip zone, a large viscosity drop on the order of 0.8 logarithmic units of viscosity causes a 25% diminishment in monitored shear stress until stabilisation associated with the self-sustainability of the process. Frictional melting in volcanic systems is finally described with its complexity in recognition in nature and its potential rheological importance during volcanic eruptions. We infer that volcanic systems (with their high temperature and pressure conditions as well as their dynamic fault/shear structures) are prone to the occurrence of frictional melting during slip events that commonly result from strain localisation in late stage magma transport.

Acknowledgements

We wish to acknowledge the help from Stefan Nielsen and Benoit Cordonnier for discussions related to the thermal correction model. We are thankful to Saskia Bernstein for assistance with the microprobe analysis, to Maurizio Petrelli for assistance with the laser ablation work, to Andrea Cavallo and Sergio Vinciguerra for preliminary imaging of the frictional glass, to Benoit Cordonnier for introducing us to the JMicroVision toolbox, and to Toshihiko Shimamoto, Wataru Tanikawa, Jackie E. Kendrick and Diego Perugini for discussion at various stage of this study. Yan Lavallée acknowledges funds from the Deutsche Forschungsgemeinschaft (DFG) grants LA 2651/1-1 and LA 2651/3-1, and Kai-Uwe Hess acknowledges the DFG grant HE 4565/2-1. Michael Heap was supported by the German Federation of Materials Science and Engineering (BV MatWerk) and the DFG. Donald B. Dingwell acknowledges support from a LMUexcellent Research Professorship in Experimental

583 Volcanology of the Bundesexzellenzinitiative as well as the Advanced Researcher
584 Grant EVOKES (247076) of the ERC. This study benefited from the constructive
585 review of an anonymous reviewer as well as John Spray.

586

587 **References**

588 Askarpour, V., Manghnani, M. H., Richet, P. 1993. Elastic properties of diopside,
589 anorthite and grossular glasses and liquids - a brillouin-scattering study up to
590 1400 K. *Journal of Geophysical Research-Solid Earth* 98(B10), 17683-17689.
591 Bagdassarov, N. S., Dingwell, D. B. 1992. A Rheological Investigation of Vesicular
592 Rhyolite. *Journal of Volcanology and Geothermal Research* 50(3), 307-322.
593 Bagdassarov, N. S., Dingwell, D. B., Webb, S. L. 1994. Viscoelasticity of Crystal-
594 Bearing and Bubble-Bearing Rhyolite Melts. *Physics of the Earth and*
595 *Planetary Interiors* 83(2), 83-99.
596 Bornhoft, H., Brückner, R. 1994. Ultrasonic measurements and complex elastic-
597 moduli of silicate glass melts in the viscoelastic and viscous range.
598 *Glastechnische Berichte-Glass Science and Technology* 67(9), 241-254.
599 Bottinga, Y., Weill, D. F. 1972. Viscosity of Magmatic Silicate Liquids - Model for
600 Calculation. *American Journal of Science* 272(5), 438-&.
601 Bower, S. M., Woods, A. W. 1996. On the dispersal of clasts from volcanic craters
602 during small explosive eruptions. *Journal of Volcanology and Geothermal*
603 *Research* 73(1-2), 19-32.
604 Brückner, R., Yue, Y. Z. 1994. Non-Newtonian Flow Behavior of Glass Melts as a
605 Consequence of Viscoelasticity and Anisotropic Flow. *Journal of Non-*
606 *Crystalline Solids* 175(2-3), 118-128.
607 Caricchi, L., Burlini, L., Ulmer, P., Gerya, T., Vassalli, M., Papale, P. 2007. Non-
608 Newtonian rheology of crystal-bearing magmas and implications for magma
609 ascent dynamics. *Earth and Planetary Science Letters* 264, 402-419.
610 Cashman, K. V., Thornber, C. R., Pallister, J. S. 2008. From Dome to Dust: Shallow
611 Crystallization and Fragmentation of Conduit Magma During the 2004-2006
612 Dome Extrusion of Mount St. Helens, Washington. In: *A Volcano Rekindled:*
613 *The Renewed Eruption of Mount St. Helens, 2004-2006* (edited by Sherrod, D.
614 R., Scott, W. E. & Stauffer, P. H.). Professionnal Paper 1750. U.S. Geological
615 Survey, 387-413.
616 Cimarelli, C., Costa, A., Mueller, S., Mader, H. M. 2011. Rheology of magmas with
617 bimodal crystal size and shape distributions: Insights from analog
618 experiments. *Geochemistry Geophysics Geosystems* 12(Q07024), 14pp.
619 Cordonnier, B., Hess, K. U., Lavallee, Y., Dingwell, D. B. 2009. Rheological
620 properties of dome lavas: a case study of Unzen. *Earth and Planetary Science*
621 *Letters*.
622 Cordonnier, B., Schmalholz, S. M., Hess, K. U., Dingwell, D. B. in press. Viscous
623 heating in silicate melts: an experimental and numerical comparison. *Journal*
624 *of Geophysical Research*.
625 Costa, A., Caricchi, L., Bagdassarov, N. 2009. A model for the rheology of particle-
626 bearing suspensions and partially molten rocks. *Geochemistry Geophysics*
627 *Geosystems* 10.

628 Costa, A., Melnik, O., Sparks, R. S. J., Voight, B. 2007. Control of magma flow in
629 dykes on cyclic lava dome extrusion. *Geophysical Research Letters* 34(2).
630 Cowan, D. S. 1999. Do faults preserve a record of seismic slip? A field geologist's
631 opinion. *Journal of Structural Geology* 21(8-9), 995-1001.
632 Cranmer, D., Uhlmann, D. R. 1981. Viscosity of Liquid Albite, a Network Material.
633 *Journal of Non-Crystalline Solids* 45(2), 283-288.
634 Cukierman, M., Uhlmann, D. R. 1973. Viscosity of Liquid Anorthite. *Journal of*
635 *Geophysical Research* 78(23), 4920-4923.
636 Del Gaudio, P., Di Toro, G., Han, R., Hirose, T., Nielsen, S., Shimamoto, T., Cavallo,
637 A. 2009. Frictional melting of peridotite and seismic slip. *Journal of*
638 *Geophysical Research-Solid Earth* 114.
639 Di Toro, G., Han, R., Hirose, T., De Paola, N., Nielsen, S., Mizoguchi, K., Ferri, F.,
640 Cocco, M., Shimamoto, T. 2011. Fault lubrication during earthquakes. *Nature*
641 471(7339), 494-+.
642 Di Toro, G., Hirose, T., Nielsen, S., Pennacchioni, G., Shimamoto, T. 2006a. Natural
643 and experimental evidence of melt lubrication of faults during earthquakes.
644 *Science* 311(5761), 647-649.
645 Di Toro, G., Hirose, T., Nielsen, S., Shimamoto, T. 2006b. Relating high-velocity
646 rock-friction experiments to coseismic slip in the presence of melts.
647 *Earthquakes: Radiated Energy and the Physics of Faulting* 170, 121-134.
648 Dingwell, D. B. 1991. Redox Viscometry of Some Fe-Bearing Silicate Melts.
649 *American Mineralogist* 76(9-10), 1560-1562.
650 Dingwell, D. B. 2007. Diffusion, viscosity and flow of melts. In: *Mineral Physics*
651 (edited by Price, G. D.). *Treatise in Geophysics* 2. Elsevier, Amsterdam, 419-
652 436.
653 Dingwell, D. B., Hess, K. U. 1998. Melt viscosities in the system Na-Fe-Si-O-F-Cl:
654 Contrasting effects of F and Cl in alkaline melts. *American Mineralogist* 83(9-
655 10), 1016-1021.
656 Dingwell, D. B., Holtz, F., Behrens, H. 1997. The solubility of H2O in peralkaline
657 and peraluminous granitic melts. *American Mineralogist* 82(3-4), 434-437.
658 Dingwell, D. B., Romano, C., Hess, K. U. 1996. The effect of water on the viscosity
659 of a haplogranitic melt under P-T-X conditions relevant to silicic volcanism.
660 *Contributions to Mineralogy and Petrology* 124(1), 19-28.
661 Dingwell, D. B., Scarfe, C. M., Cronin, D. J. 1985. The Effect of Fluorine on
662 Viscosities in the System Na2o-Al2o3-Sio2 - Implications for Phonolites,
663 Trachytes and Rhyolites. *American Mineralogist* 70(1-2), 80-87.
664 Dingwell, D. B., Webb, S. L. 1989. Structural relaxation in silicate melts and non-
665 Newtonian melt rheology in geologic processes. *Physics and Chemistry of*
666 *Minerals* 16(5), 508-516.
667 Dingwell, D. B., Webb, S. L. 1990. Relaxation in silicate melts. *European Journal of*
668 *Mineralogy* 2(4), 427-449.
669 Einstein, A. 1906. A new determination of the molecular dimensions. *Annalen Der*
670 *Physik* 19(2), 289-306.
671 Einstein, A. 1911. A new determination of the molecular dimensions (vol 19, pg 289,
672 1906). *Annalen Der Physik* 34(3), 591-592.
673 Giordano, D., Russell, J. K., Dingwell, D. B. 2008. Viscosity of magmatic liquids: A
674 model. *Earth and Planetary Science Letters* 271, 123-134.
675 Gonnermann, H. M., Manga, M. 2007. The fluid mechanics inside a volcano. *Annual*
676 *Review of Fluid Mechanics* 39, 321-356.

677 Gottsmann, J., Giordano, D., Dingwell, D. B. 2002. Predicting shear viscosity during
678 volcanic processes at the glass transition: a calorimetric calibration. *Earth and*
679 *Planetary Science Letters* 198(3-4), 417-427.
680 Grunewald, U., Sparks, R. S. J., Kearns, S., Komorowski, J. C. 2000. Friction marks
681 on blocks from pyroclastic flows at the Soufriere Hills volcano, Montserrat:
682 Implications for flow mechanisms. *Geology* 28(9), 827-830.
683 Hess, K. U., Cordonnier, B., Lavallée, Y., Dingwell, D. B. 2008. Viscous heating in
684 rhyolite: an in situ determination. *Earth and Planetary Science Letters* 275(1-
685 2), 121-126.
686 Hess, K. U., Dingwell, D. B. 1996. Viscosities of hydrous leucogranitic melts: A non-
687 Arrhenian model. *American Mineralogist* 81(9-10), 1297-1300.
688 Hessenkemper, H., Brückner, R. 1991. Elastic constants of glass melts above the
689 glass-transition temperature from ultrasonic and axial-compression
690 measurements. *Glastechnische Berichte-Glass Science and Technology* 64(2),
691 29-38.
692 Hirose, T., Shimamoto, T. 2005. Growth of molten zone as a mechanism of slip
693 weakening of simulated faults in gabbro during frictional melting. *Journal of*
694 *Geophysical Research-Solid Earth* 110(B5).
695 Hui, H. J., Zhang, Y. X. 2007. Toward a general viscosity equation for natural
696 anhydrous and hydrous silicate melts. *Geochimica Et Cosmochimica Acta*
697 71(2), 403-416.
698 Iverson, R. M., Dzurisin, D., Gardner, C. A., Gerlach, T. M., LaHusen, R. G.,
699 Lisowski, M., Major, J. J., Malone, S. D., Messerich, J. A., C., M. S., Pallister,
700 J. S., Qamar, A. I., Schilling, S. P., Vallance, J. W. 2006. Dynamics of
701 seismogenic volcanic extrusion at Mount St Helens in 2004-05. *Geology* 444,
702 439-443.
703 Johnson, J. B., Lees, J. M., Gerst, A., Sahagian, D., Varley, N. 2008. Long-period
704 earthquakes and co-eruptive dome inflation seen with particle image
705 velocimetry. *Nature* 456(7220), 377-381.
706 Kendrick, J. E., Lavallée, Y., Ferk, A., Perugini, D., Leonhardt, R., Dingwell, D. B.
707 this issue. Extreme frictional processes in the volcanic conduit of Mount St.
708 Helens (USA) during the 2004-2008 eruption. *Journal of Structural Geology*.
709 Kennedy, L. A., Russell, J. K. 2011. Cataclastic Production of Volcanic Ash at Mount
710 Saint Helens. *Chemistry and Physics of the Earth*.
711 Kennedy, L. A., Russell, J. K., Nelles, E. 2009. Origins of Mount St. Helens
712 cataclasites: Experimental insights. *American Mineralogist* 94(7), 995-1004.
713 Kennedy, L. A., Spray, J. G. 1992. Frictional melting of sedimentary-rock during
714 high-speed diamond drilling - an analytical SEM and TEM investigation.
715 *Tectonophysics* 204(3-4), 323-337.
716 Kim, J. W., Ree, J. H., Han, R., Shimamoto, T. 2010. Experimental evidence for the
717 simultaneous formation of pseudotachylyte and mylonite in the brittle regime.
718 *Geology* 38(12), 1143-1146.
719 Kokelaar, P. 2007. Friction melting, catastrophic dilation and breccia formation along
720 caldera superfaults. *Journal of the Geological Society* 164, 751-754.
721 Labaš, M., Krepelka, F., Miklúšová, V. 2006. Complex investigation of thermo-
722 technical parameters of Ruskov andesite. *Acta Montanistica Slovaca* 11, 321-
723 325.
724 Lavallée, Y., Hess, K. U., Cordonnier, B., Dingwell, D. B. 2007. A non-Newtonian
725 rheological law for highly-crystalline dome lavas. *Geology* 35, 843-846.

726 Lavallée, Y., Meredith, P., Dingwell, D. B., Hess, K. U., Wassermann, J., Cordonnier,
727 B., Gerik, A., Kruhl, J. H. 2008. Seismogenic lavas and explosive eruption
728 forecasting. *Nature* 453(22 May), 507-510.
729 Legros, F., Cantagrel, J. M., Devouard, B. 2000. Pseudotachylyte (frictionite) at the
730 base of the Arequipa volcanic landslide deposit (Peru): Implications for
731 emplacement mechanisms. *Journal of Geology* 108(5), 601-611.
732 Lejeune, A. M., Bottinga, Y., Trull, T. W., Richet, P. 1999. Rheology of bubble-
733 bearing magmas. *Earth and Planetary Science Letters* 166(1-2), 71-84.
734 Lejeune, A. M., Richet, P. 1995. Rheology of Crystal-Bearing Silicate Melts - an
735 Experimental-Study at High Viscosities. *Journal of Geophysical Research-*
736 *Solid Earth* 100(B3), 4215-4229.
737 Li, J. H., Uhlmann, D. R. 1968. Flow of Glass at High Stress Levels. *American*
738 *Ceramic Society Bulletin* 47(4), 402-&.
739 Li, J. H., Uhlmann, D. R. 1970. The flow of glass at high stress levels : I. Non-
740 Newtonian behavior of homogeneous 0.08 Rb2O[middle dot]0.92 SiO2
741 glasses. *Journal of Non-Crystalline Solids* 3(1), 127-147.
742 Liebske, C., Behrens, H., Holtz, F., Lange, R. A. 2003. The influence of pressure and
743 composition on the viscosity of andesitic melts. *Geochimica Et Cosmochimica*
744 *Acta* 67(3), 473-485.
745 Lin, A. M., Shimamoto, T. 1998. Selective melting processes as inferred from
746 experimentally generated pseudotachylytes. *Journal of Asian Earth Sciences*
747 16(5-6), 533-545.
748 Malfait, W. J., Sanchez-Valle, C., Ardia, P., Medard, E., Lerch, P. 2011.
749 Compositional dependent compressibility of dissolved water in silicate
750 glasses. *American Mineralogist* 96(8-9), 1402-1409.
751 McKenzie, D., Brune, J. N. 1972. Melting of fault planes during large earthquakes.
752 *Geophysical Journal of the Royal Astronomical Society* 29(1), 65-&.
753 Melnik, O., Sparks, R. S. J. 1999. Nonlinear dynamics of lava dome extrusion. *Nature*
754 402(6757), 37-41.
755 Melnik, O., Sparks, R. S. J., Costa, A., Barmin, A. A. 2009. Volcanic eruptions:
756 Cyclicity during lava dome growth. In: *Encyclopedia of Complexity and*
757 *Systems Science* (edited by Meyers, R. A.). Springer, 9763-9784
758 Mezic, I., Brady, J. F., Wiggins, S. 1996. Maximal effective diffusivity for time
759 periodic incompressible fluid flows. *Journal of Applied Mathematics* 56, 40-
760 57.
761 Murase, T., McBirney, A. R. 1970. Viscosity of Lunar Lavas. *Science* 167(3924),
762 1491-&.
763 Nakamura, N., Hirose, T., Borradaile, G. J. 2002. Laboratory verification of
764 submicron magnetite production in pseudotachylytes: relevance for
765 paleointensity studies. *Earth and Planetary Science Letters* 201(1), 13-18.
766 Neuberg, J. W., Tuffen, H., Collier, L., Green, D., Powell, T., Dingwell, D. 2006. The
767 trigger mechanism of low-frequency earthquakes on Montserrat. *Journal of*
768 *Volcanology and Geothermal Research* 153(1-2), 37-50.
769 Neuville, D. R., Richet, P. 1991. Viscosity and Mixing in Molten (Ca, Mg) Pyroxenes
770 and Garnets. *Geochimica Et Cosmochimica Acta* 55(4), 1011-1019.
771 Nielsen, S., Di Toro, G., Hirose, T., Shimamoto, T. 2008. Frictional melt and seismic
772 slip. *Journal of Geophysical Research-Solid Earth* 113(B1).
773 Niemeijer, A., Di Toro, G., Nielsen, S., Di Felice, F. 2011. Frictional melting of
774 gabbro under extreme experimental conditions of normal stress, acceleration,
775 and sliding velocity. *Journal of Geophysical Research-Solid Earth* 116.

776 Persikov, E. S., Zharikov, V. A., Bukhtiyarov, P. G., Polskoy, S. F. 1990. The Effect
777 of Volatiles on the Properties of Magmatic Melts. *European Journal of*
778 *Mineralogy* 2(5), 621-642.
779 Perugini, D., Poli, G. 2004. Analysis and numerical simulation of chaotic advection
780 and chemical diffusion during magma mixing: petrological implications.
781 *Lithos* 78(1-2), 43-66.
782 Perugini, D., Poli, G., Petrelli, M., De Campos, C. P., Dingwell, D. B. 2010. Time-
783 Scales of Recent Phlegrean Fields Eruptions Inferred from the Application of
784 a 'Diffusive Fractionation' Model of Trace Elements. *Bulletin of Volcanology*
785 72, 431-447.
786 Piccardo, G. B., Ranalli, G., Guarnieri, L. 2010. Seismogenic Shear Zones in the
787 Lithospheric Mantle: Ultramafic Pseudotachylytes in the Lanzo Peridotite
788 (Western Alps, NW Italy). *Journal of Petrology* 51(1-2), 81-100.
789 Ramos, J. I. 1995. One-dimensional, time-dependent, homogeneous, 2-phase flow in
790 volcanic conduits. *International Journal for Numerical Methods in Fluids*
791 21(3), 253-278.
792 Reubi, O., Blundy, J. 2008. Assimilation of Plutonic Roots, Formation of High-K
793 Exotic Melt Inclusions and Genesis of Andesitic Magmas at Volcán De
794 Colima, Mexico. *Journal of Petrology* 49(12), 2221-2243.
795 Rice, J. R. 2006. Heating and weakening of faults during earthquake slip. *Journal of*
796 *Geophysical Research-Solid Earth* 111(B5).
797 Richet, P. 1984. Viscosity and Configurational Entropy of Silicate Melts. *Geochimica*
798 *Et Cosmochimica Acta* 48(3), 471-483.
799 Richet, P., Lejeune, A. M., Holtz, F., Roux, J. 1996. Water and the viscosity of
800 andesite melts. *Chemical Geology* 128(1-4), 185-197.
801 Roduit, N. 2006. JMicroVision: Image analysis toolbox for measuring and
802 quantifying components of high-definition images.
803 Roscoe, R. 1952. The Viscosity of Suspensions of Rigid Spheres. *British Journal of*
804 *Applied Physics* 3(AUG), 267-269.
805 Sato, H. 2005. Viscosity measurement of subliquidus magmas: 1707 basalt of Fuji
806 volcano. *Journal of Mineralogical and Petrological Sciences* 100(4), 133-142.
807 Sato, K., Kumagai, H., Hirose, T., Tamura, H., Mizoguchi, K., Shimamoto, T. 2009.
808 Experimental study for noble gas release and exchange under high-speed
809 frictional melting. *Chemical Geology* 266(1-2), 96-103.
810 Savov, I. P., Luhr, J. F., Navarro-Ochoa, C. 2008. Petrology and geochemistry of lava
811 and ash erupted from Volcan Colima, Mexico, during 1998-2005. *Journal of*
812 *Volcanology and Geothermal Research* 174(4), 241-256.
813 Scaillet, B., Holtz, F., Pichavant, M., Schmidt, M. 1996. Viscosity of Himalayan
814 leucogranites: Implications for mechanisms of granitic magma ascent. *Journal*
815 *of Geophysical Research-Solid Earth* 101(B12), 27691-27699.
816 Schilling, F. R., Hauser, M., Sinogeikin, S. V., Bass, J. D. 2001. Compositional
817 dependence of elastic properties and density of glasses in the system anorthite-
818 diopside-forsterite. *Contributions to Mineralogy and Petrology* 141(3), 297-
819 306.
820 Schulze, F., Behrens, H., Hurkuck, W. 1999. Determination of the influence of
821 pressure and dissolved water on the viscosity of highly viscous melts:
822 Application of a new parallel-plate viscometer. *American Mineralogist* 84(10),
823 1512-1520.

824 Schwarzkopf, L. M., Schmincke, H. U., Troll, V. R. 2001. Pseudotachylite on impact
825 marks of block surfaces in block-and-ash flows at Merapi volcano, Central
826 Java, Indonesia. *International Journal of Earth Sciences* 90(4), 769-775.
827 Shaw, H. R. 1972. Viscosities of Magmatic Silicate Liquids - Empirical Method of
828 Prediction. *American Journal of Science* 272(9), 870-&.
829 Shimamoto, T., Lin, A. M. 1994. Is frictional melting equilibrium or non-equilibrium
830 melting? *Structural Geology (Journal of the Tectonic Research Group of*
831 *Japan)* 39, 79-84.
832 Sibson, R. H. 1975. Generation of pseudotachylyte by ancient seismic faulting.
833 *Geophysical Journal of the Royal Astronomical Society* 43(3), 775-&.
834 Simmons, J. H. 1998. Morey Award paper - What is so exciting about non-linear
835 viscous flow in glass, molecular dynamics simulations of brittle fracture and
836 semiconductor-glass quantum composites. *Journal of Non-Crystalline Solids*
837 239(1-3), 1-15.
838 Simmons, J. H., Mohr, R. K., Montrose, C. J. 1982. Viscous Failure of Glass at High
839 Shear Rates. *Journal De Physique* 43(NC-9), 439-442.
840 Simmons, J. H., Ochoa, R., Simmons, K. D., Mills, J. J. 1988. Non-Newtonian
841 Viscous-Flow in Soda-Lime Silica Glass at Forming and Annealing
842 Temperatures. *Journal of Non-Crystalline Solids* 105(3), 313-322.
843 Sparks, R. S. J. 2003. Forecasting volcanic eruptions. *Earth and Planetary Science*
844 *Letters* 210(1-2), 1-15.
845 Spray, J. G. 1987. Artificial generation of pseudotachylyte using friction welding
846 apparatus - simulation on a fault plane. *Journal of Structural Geology* 9(1),
847 49-60.
848 Spray, J. G. 1988. Generation and crystallization of an amphibolite shear melt - an
849 investigation using radial friction welding apparatus. *Contributions to*
850 *Mineralogy and Petrology* 99(4), 464-475.
851 Spray, J. G. 1992. A physical basis for the frictional melting of some rock-forming
852 minerals. *Tectonophysics* 204(3-4), 205-221.
853 Spray, J. G. 1993. Viscosity determination of some frictionally generated silicate
854 melts - Implications for fault zone rheology at high strain rates. *Journal of*
855 *Geophysical Research-Solid Earth* 98(B5), 8053-8068.
856 Spray, J. G. 1995. Pseudotachylyte controversy - fact of friction. *Geology* 23(12),
857 1119-1122.
858 Stein, D. J., Spera, F. J. 1992. Rheology and Microstructure of Magmatic Emulsions -
859 Theory and Experiments. *Journal of Volcanology and Geothermal Research*
860 49(1-2), 157-174.
861 Stein, D. J., Spera, F. J. 2002. Shear viscosity of rhyolite-vapor emulsions at
862 magmatic temperatures by concentric cylinder rheometry. *Journal of*
863 *Volcanology and Geothermal Research* 113(1-2), 243-258.
864 Stevenson, R. J., Dingwell, D. B., Webb, S. L., Sharp, T. G. 1996. Viscosity of
865 microlite-bearing rhyolitic obsidians: An experimental study. *Bulletin of*
866 *Volcanology* 58(4), 298-309.
867 Taniguchi, H. 1992. Entropy Dependence of Viscosity and the Glass-Transition
868 Temperature of Melts in the System Diopside-Anorthite. *Contributions to*
869 *Mineralogy and Petrology* 109(3), 295-303.
870 Tauber, P., Arndt, J. 1987. The Relationship between Viscosity and Temperature in
871 the System Anorthite Diopside. *Chemical Geology* 62(1-2), 71-81.

Toplis, M. J., Dingwell, D. B., Hess, K. U., Lenci, T. 1997. Viscosity, fragility, and configurational entropy of melts along the join SiO2-NaAlSiO4. *American Mineralogist* 82(9-10), 979-990.

Tsutsumi, A., Mizoguchi, K. 2007. Effect of melt squeezing rate on shear stress along a simulated fault in gabbro during frictional melting. *Geophysical Research Letters* 34(21), 5.

Tsutsumi, A., Shimamoto, T. 1997. High-velocity frictional properties of gabbro. *Geophysical Research Letters* 24(6), 699-702.

Tuffen, H., Dingwell, D. B., Pinkerton, H. 2003. Repeated fracture and healing of silicic magma generate flow banding and earthquakes? *Geology* 31(12), 1089-1092.

Tuffen, H., Smith, R., Sammonds, P. R. 2008. Evidence for seismogenic fracture of silicic magma. *Nature* 453(7194), 511-514.

Ujiie, K., Tsutsumi, A., Fialko, Y., Yamaguchi, H. 2009. Experimental investigation of frictional melting of argillite at high slip rates: Implications for seismic slip in subduction-accretion complexes. *Journal of Geophysical Research-Solid Earth* 114.

Ujiie, K., Yamaguchi, H., Sakaguchi, A., Toh, S. 2007. Pseudotachylytes in an ancient accretionary complex and implications for melt lubrication during subduction zone earthquakes. *Journal of Structural Geology* 29(4), 599-613.

Vo-Thanh, D., Bottinga, Y., Polian, A., Richet, P. 2005. Sound velocity in alumino-silicate liquids determined up to 2550 K from Brillouin spectroscopy: glass transition and crossover temperatures. *Journal of Non-Crystalline Solids* 351(1), 61-68.

Webb, S. L. 1991. Shear and volume relaxation in $Na_2Si_2O_5$. *American Mineralogist* 76(9-10), 1449-1454.

Webb, S. L., Dingwell, D. B. 1990. The Onset of Non-Newtonian Rheology of Silicate Melts - a Fiber Elongation Study. *Physics and Chemistry of Minerals* 17(2), 125-132.

Wilson, L., Sparks, R. S. J., Walker, G. P. L. 1980. Explosive volcanic eruptions - IV. The control of magma properties and conduit geometry on eruption column behavior. *Geophysical Journal of the Royal Astronomical Society* 63(1), 117-148.

Yue, Y. Z., Brückner, R. 1994. A New Description and Interpretation of the Flow Behavior of Glass-Forming Melts. *Journal of Non-Crystalline Solids* 180(1), 66-79.

Figure caption

Figure 1. Schematics of (a) the high-velocity rotary apparatus (as described by Hirose and Shimamoto, 2005) and (b) the sample assembly for which, four thermocouples were embayed in the sample in stationary side. 1) specimen; 2) motor; 3) torque limiter; 4) torque gauge; 5) electromagnetic clutch; 6) rotary encoder; 7) rotary column; 8) torque-axial force gauge; 9) ball spline; 10) axial force gauge; 11) air actuator; 12) displacement transducer; and 13) water reservoir.

Figure 2. Progression of shear stress and axial shortening of sample, induced by slip at a rate of 1.3 m/s and normal stress of 1 MPa. The arrow indicate the amount of slip at which incandescent bits of melts were visible. The inset shows the abrupt increase in shear stress at the onset of the experiment.

Figure 3. Frictional melt produced during slip of andesite at a slip rate of 1.3 m/s. (a) Photograph of a sample with the generated blob of frictional melt. (b) Scan of a thin section in the long axis of the sample, which highlight zone 1 (z1) in which the rock is intact; zone 2 (z2) where enough heat was generated to overcome T_g, which permitted the rock to behave viscously; and zone 3 (z3) and 4 (z4) where the rock selectively melted. Tc indicates one of the thermocouples. The accompanying microphotographs in (c) z1, (d) z2, and (e) z3 show differences in microlite contents and orientations; especially, the microlites in z2 express an increased preferred orientation of their long axis sub-parallel to the direction of shear in the slip zone (as approximated by the arrows), in contrast to z1 which display random microlite orientation. (e) viscous deformation in z3 and z4 enabled the failure and dislocation of crystal fragments.

Figure 4. (a) Mosaic of seven BSE images across the length of the slip zone. The frictional melt is visible as a lighter grey band with darker grey crystal fragments. The blue box indicates the location of figure 4c and the arrows point to the thermal cracks. (b) SEM image showing an example of protomelt forming at the interface between the rock and the frictional melt. [NOTE: this image alone was acquired with a JEOL JXA-8200 at INGV-Rome via the acknowledged assistance of A. Cavallo]. (c) BSE image of the frictional melt area in which crystal fraction was estimated using JMicrovision.

Figure 5. X-ray computed tomographic images of microstructures. [Note: the missing upper area was cut for thin section preparation] (a) plan view3 image of intact material away from the slip zone. In this area, crystals (in different shades of grey) and bubbles (in black) are homogeneously scattered. (b) Plan view image of the interface between the host rock and the slip zone. The host rock is most obvious in the center of the rock where crystal and bubble remain homogeneously scattered. In the surrounding melting zone, we observe rare, very fine crystal (most are below detection limit) and near the outer margin of the slip zone, a ring of bubbles developed. We can also see the blob of melt that spilled outside the sample and accumulated on the margin. (c) Plan view image of the slip zone. We observe annular rings in crystal size distribution (of the light Fe-oxides) as well as concentric and radial thermal cracks (see inset box). Note: the grey scale reflects the density of imaged molecules. The voxel size in the image is 36.7 microns.

Figure 6. (a) Non-Arrhenian temperature dependence of viscosity of the melts generated by frictional slip. Viscosity estimated using chemical composition as input parameter in the GRD viscosity calculator (Giordano et al., 2008). The viscosity of the frictional melt agrees well with the measured calorimetric Tg. (b) Calorimetric properties of the frictional melt during thermal analysis in a differential scanning calorimeter. The peak at a constant rate of 10 °C/min (for a known cooling rate of 10 °C/min) is used as a value of the glass transition Tg at a temperature of ~690+/-5 °C (indicated by the arrow). (c) Strain rate dependence of the relative viscosity increase induced by the presence of 30 vol.% crystal (under isothermal condition), computed using the complex viscosity model of Costa et al, 2009. (d) Evolution of the modelled temperature and the apparent viscosity of the suspension (computed for an averaged strain rate and a relative viscosity increase of 0.45 log (in Pa·s)) generated by frictional melting.

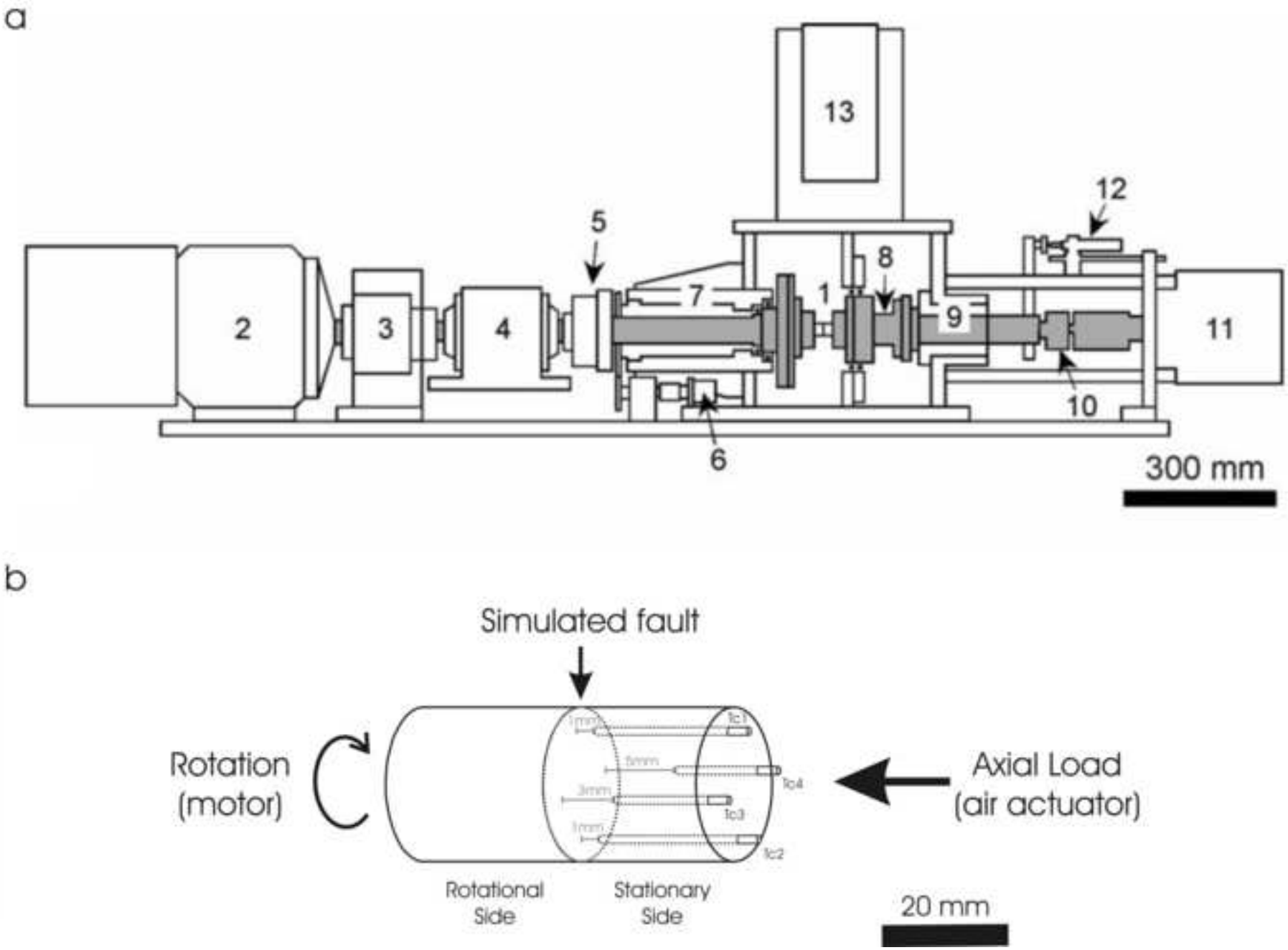

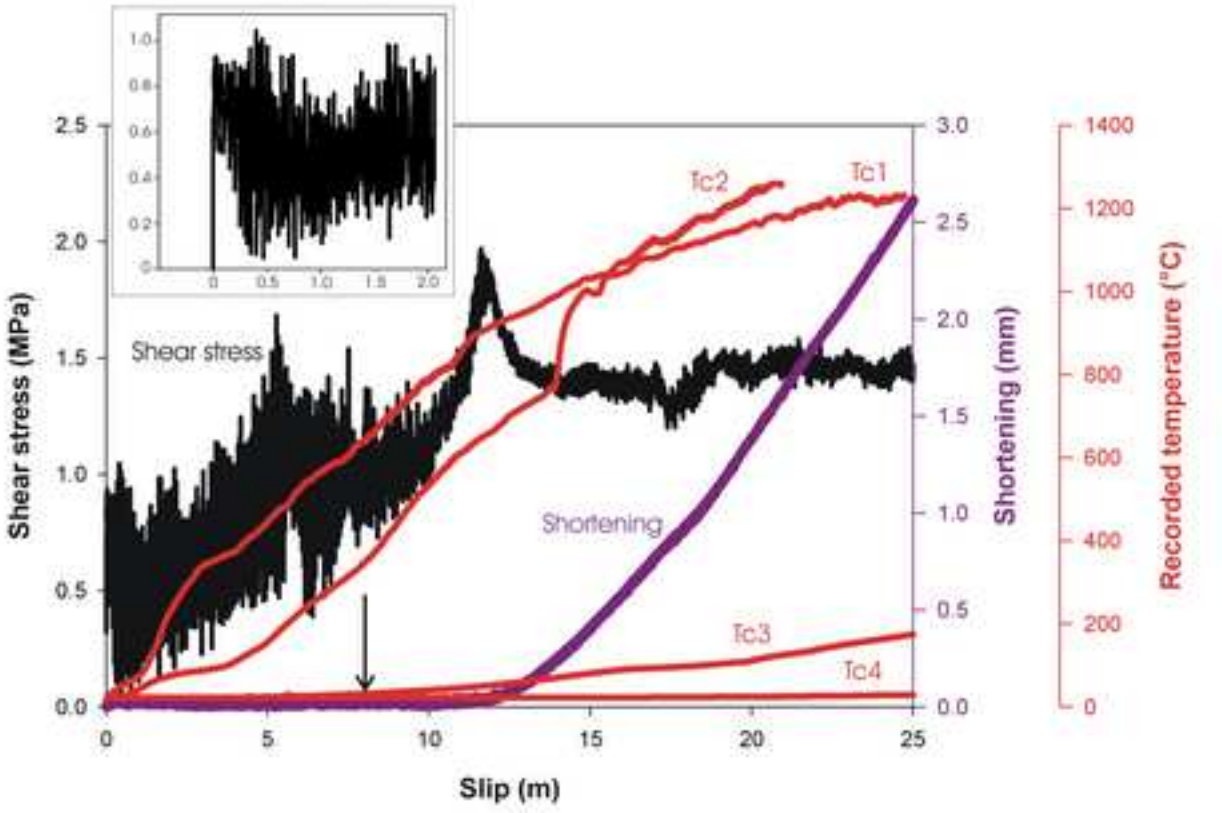

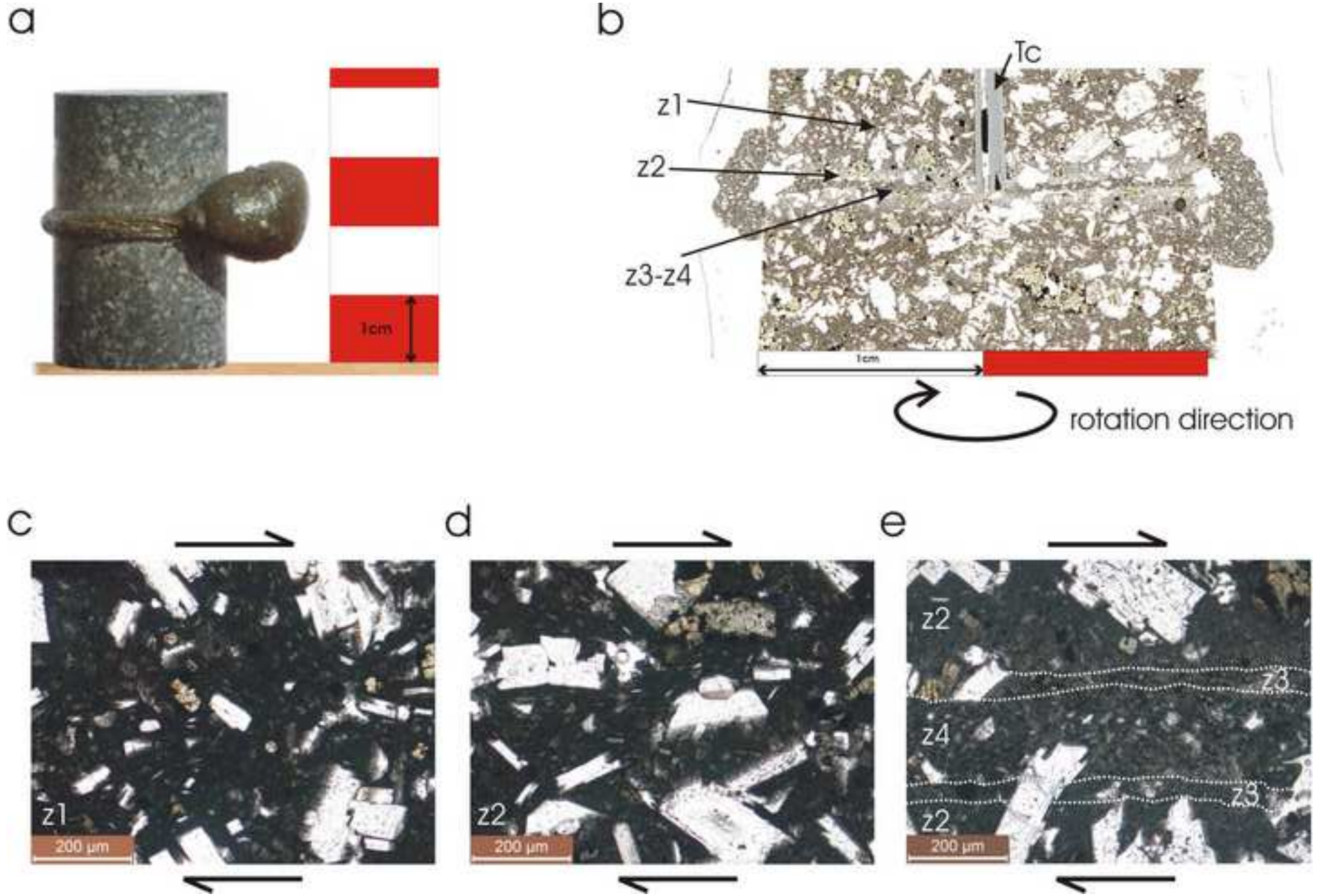

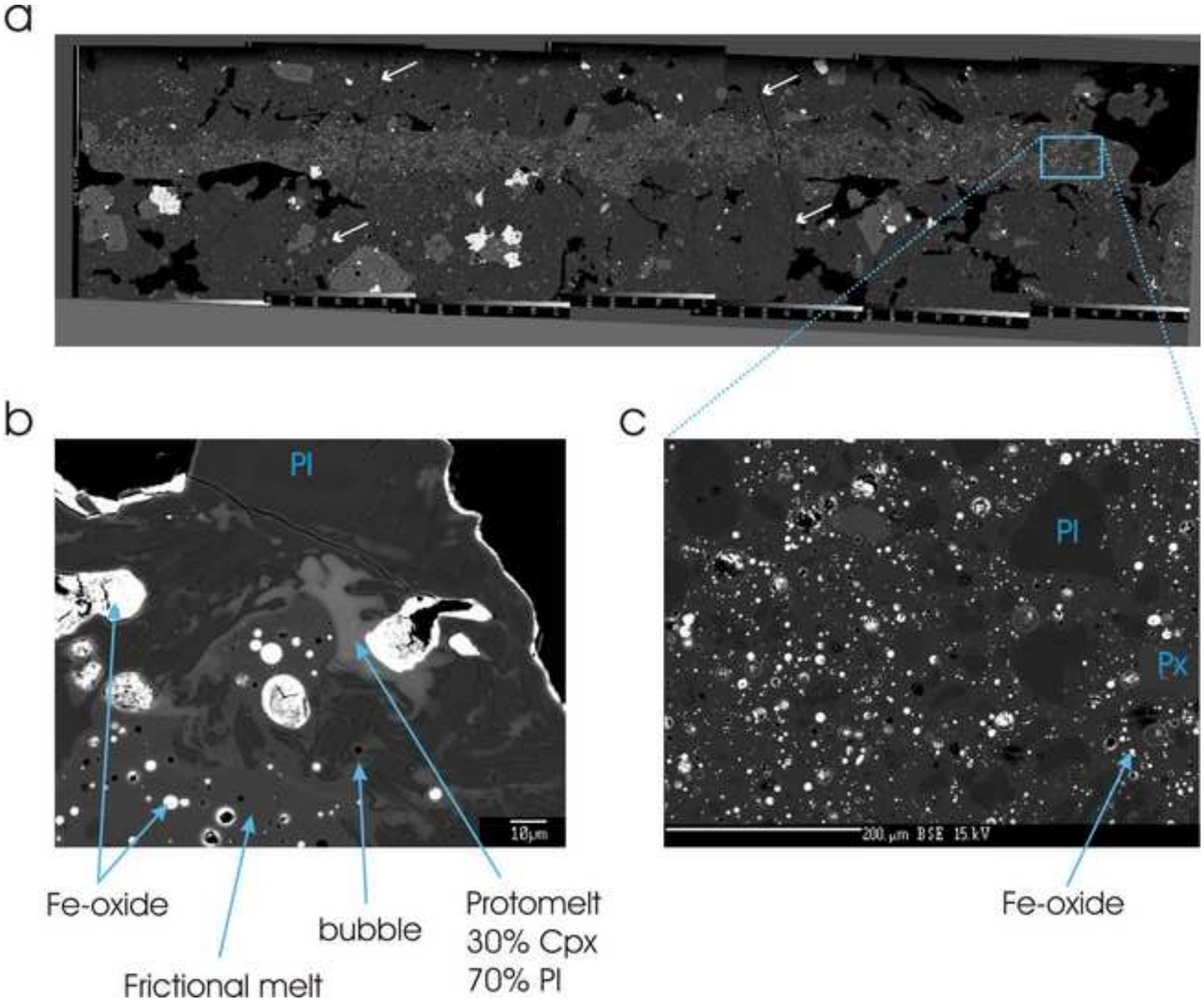

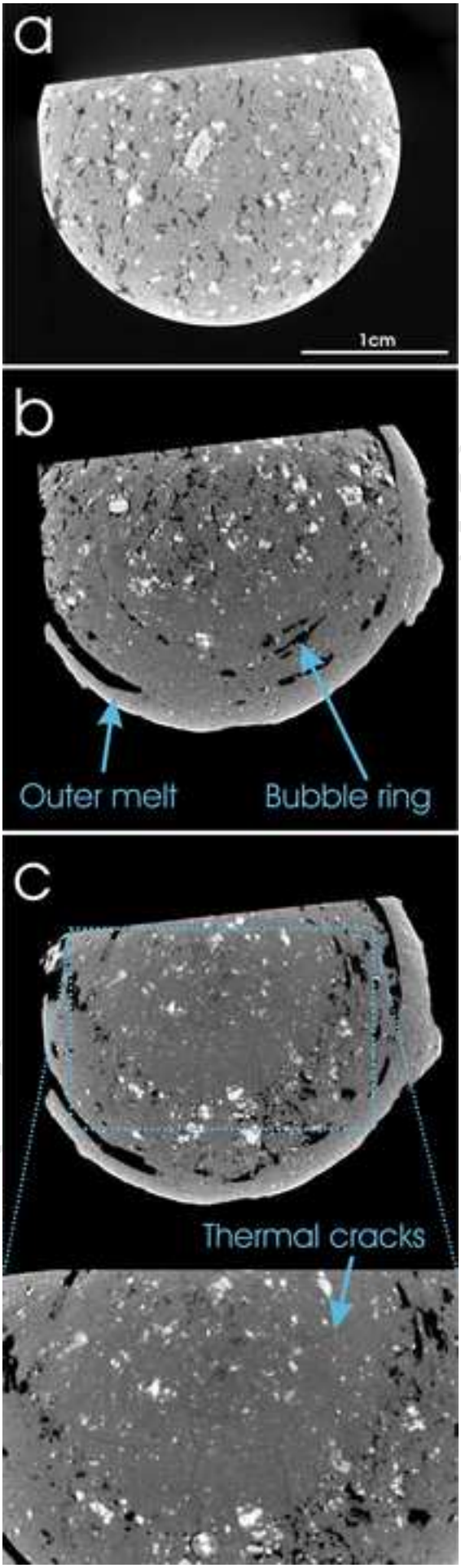

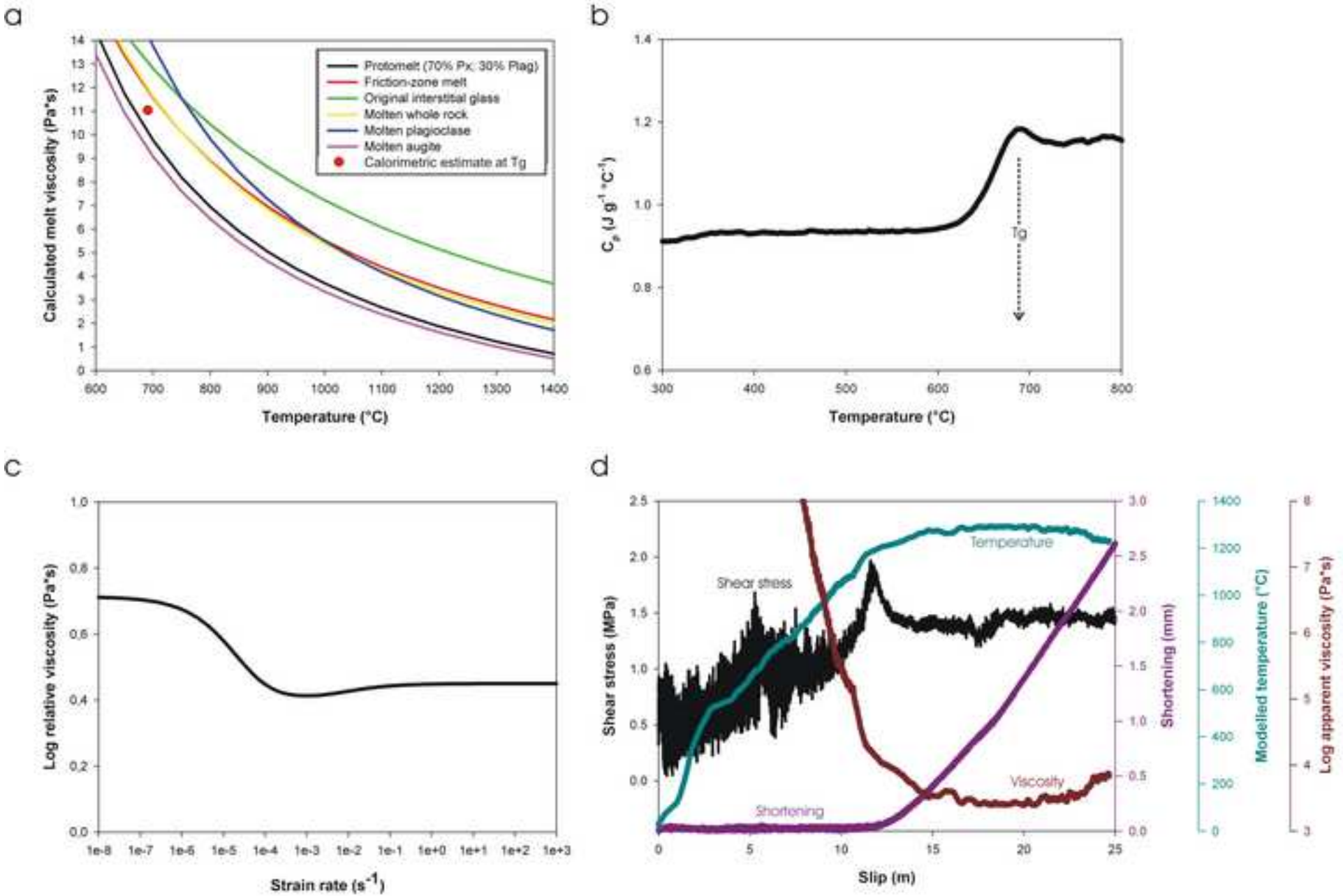

Table 1. Normalized geochemical composition of the melt generated by friction of andesite from Volcán de Colima. The compositions were measured by electron microprobe, using a 15kV beam, operating at 10 nA scanning box mode (10^2 μm^2). Standards: Si, Ca: wollastonite; Al, K: orthoclase; Na: albite; Mg: periclase; Ti, Mn: ilmenite; Fe: hematite. Std. dev.: Standard deviation.

* Bulk rock chemical composition from Reubi and Blundy, 2008

** Interstitial melt chemical composition from Lavallee et al., 2007

	Glass (69) zone #4	Glass (70) zone #4	Glass (88) zone #4	Glass (10) zone #3	Glass (11) zone #3	Glass (54) zone #3	Glass (55) zone #3	Std. dev. (sigma 1)	bulk rock*	Interstitial glass**
SiO_2	63.946	63.112	63.154	58.611	54.244	38.033	36.860	0.261	61.200	73.432
Al_2O_3	15.971	16.618	16.693	9.647	7.110	7.055	6.585	0.218	16.966	13.101
Na_2O	4.134	4.105	4.111	2.665	1.816	2.320	2.110	0.161	4.423	4.317
K_2O	1.580	1.544	1.663	1.215	0.786	0.396	0.261	0.043	1.262	3.743
MgO	2.953	2.910	3.134	6.121	8.607	8.107	8.377	0.174	3.898	0.376
CaO	5.207	5.396	5.341	8.162	10.044	12.172	13.624	0.159	6.100	1.408
TiO_2	0.633	0.672	0.597	0.977	1.303	2.177	2.523	0.041	0.596	0.745
FeO	5.274	5.260	4.985	10.732	13.204	19.893	18.402	0.258	5.272	2.588
MnO	0.100	0.125	0.130	0.337	0.379	0.452	0.514	0.042	0.101	0.071
P_2O_5	0.202	0.257	0.190	1.533	2.507	9.396	10.743	0.103	0.182	0.220